Check for updates

Visualization of pore water colloids in intact soil using a new diffusive gradients in thin films (DGT)-based approach

Claudia Moens, [iD] *[a] Justin Payne,[b] Casey L. Doolette,[b] Camille Resseguier,[e]
Jan Vanderborght, [iD] [ad] Enzo Lombi[c] and Erik Smolders[a]

Mobile colloids, most notably natural nanoparticles (NP) within the <100 nm range, enhance the mobility of nutrients and contaminants in soil; however, unbiased sampling methods are lacking to properly quantify colloid-facilitated transport. We advanced the imaging diffusive gradients in thin films (DGT) method to sample not only solutes but also pore water colloids in intact soils. The DGT setup consisted of a zirconium oxide–Chelex binding layer separated from soil by a 9 μm thick membrane with a pore size of 1 μm, providing a short diffusion length to increase colloid sensitivity. The method was tested in a vertical 15 cm section near the plough pan at about 30 cm depth in an arable soil (Luvisol) with silt-loam texture. Intact soil cores were sampled, sliced along the longitudinal axis, and the DGT was deployed on the exposed surface. Two-dimensional mapping of the DGT by LA-Time-of-Flight (TOF)-MS identified striking co-localisation of Al, Si, Rb, and Cs, indicating clay colloids. Pore water extracted from the same soil cores and analysed using Flow Field Flow Fractionation confirmed 2 : 1 clay minerals as the dominant colloids. Laboratory studies confirmed the potential of the DGT binding layer to concentrate clay colloids from suspensions, likely due to cation bridging between the negatively charged clay surfaces and the zirconium oxide in the binding layer. Colloids were present on the soil-deployed gels primarily at locations where pore water Ca^{2+} concentrations were lower, likely corresponding to larger pores that were mostly drained at the time of sampling. This study presents the first 2D map of pore water colloids in soil, future work will focus on converting DGT data into resident colloid concentrations.

Environmental significance

This study presents a novel DGT-based method for in situ sampling of pore water colloids in intact cores, overcoming artefacts of conventional bulk sampling. Innovations in the DGT setup include a thin (9 μm), large-pore (1 μm) membrane and a zirconium oxide–Chelex binding layer, enabling sensitive colloid collection while preserving soil heterogeneity. Coupled with high-resolution LA-TOF-MS and synchrotron-XFM, the method produced the first high-resolution 2D maps of pore water colloids in soil. By enabling in situ, spatially resolved measurements of pore water colloids in soil, this method opens opportunities for improved prediction of nutrient and contaminant mobility in agricultural and contaminated soils.

Introduction

Individual particles of clay, silt, and sand are organised in soil into larger aggregates, forming pores of various sizes that

[a] Division of Soil and Water Management, KU Leuven, Kasteelpark Arenberg 20, 3001 Heverlee, Belgium. E-mail: claudia.moens@kuleuven.be, erik.smolders@kuleuven.be
[b] Adelaide University, Mawson Lakes, South Australia 5095, Australia. E-mail: justin.payne@adelaide.edu.au, casey.doolette@adelaide.edu.au
[c] Future Industries Institute, Adelaide University, Mawson Lakes, South Australia 5095, Australia. E-mail: e.lombi@adelaide.edu.au
[d] Agrosphere Institute, IBG-3, Forschungszentrum Jülich, Germany. E-mail: j.vanderborght@fz-juelich.de
[e] Université Paris-Saclay, INRAE, AgroParisTech, UMR EcoSys, 91120 Palaiseau, France. E-mail: Camille.Resseguier@inrae.fr

define the soil's structure. These soil aggregates are composed of organo-mineral associations in which organic matter, clay minerals, and iron (Fe) and aluminum (Al) (hydr) oxides act as binding agents[1] and strongly retain nutrients and contaminants in soil. The resulting pore structure governs water and solute transport. Macropores (>60 μm) facilitate rapid, non-equilibrium flow that bypasses the soil matrix, mesopores (60 to 0.2 μm) enable slower, diffusion-driven transport, while micropores retain water strongly, prolonging solute-soil interaction times.[2] Conventional soil chemical analyses, however, typically disrupt the soil structure by air-drying, and sieving the soil prior to batch extraction, most commonly based on intensive agitation. These batch extraction methods, while practical, break down

This journal is © The Royal Society of Chemistry 2026

Environ. Sci.: Nano, 2026, **13**, 1935–1947 | 1935

aggregates and pore structure, thereby exposing more reactive surfaces than would normally be available in intact soil, potentially misrepresenting the mobility of nutrients and contaminants. Therefore, there is a need for sampling methods that preserve soil structure, though such approaches remain limited.

The components in pore water can occur as dissolved molecular species or as mobile colloids, typically defined as particles ranging from the nanometre to the micrometre scale (≈ 1 nm–1 µm). Within this size continuum, the smallest reactive fraction (<100 nm) is commonly referred to as natural nanoparticles and includes clay minerals, soil organic matter, and amorphous Fe and Al (oxyhydr)oxide clusters. These nanosized particles act as highly reactive nanovectors that facilitate the mobilisation and transport of associated nutrients and contaminants.[3] It is well established that such colloids can be the major mobile carriers for strongly sorbing elements such as metals,[4] radionuclides[5] and oxyanions in soils.[6] For example, various column and field studies found that mobile soil colloids can enhance nutrient (*e.g.* phosphate) leaching in soil.[6–9]

The contribution of colloid-facilitated transport on the long-term mobility of elements in intact soils remains uncertain because the risk of creating artefacts is significant when sampling pore water colloids from intact soil. The commonly employed centrifugation methods and suction cup methods tend to underestimate colloid concentrations because they either compact the soil during centrifugation or use filters that trap colloids through straining.[10] Soil extraction techniques alter the soil structure during shaking, potentially releasing colloids, and such techniques rarely sample solution at equal ionic strength as that of the *in situ* solution. *In situ* sampling methods of intact soil using suction plates, rhizon samplers, and wick lysimeters preserve the limited exchange between mobile and immobile water during leaching.[11] However, they typically underestimate colloids due to trapping of the colloids on the plates[4,12] or onto the wicks.[13]

The DGT technique allows *in situ* sampling of solutes in intact soil.[14] The method consists of a binding layer (BL) that acts as a zero-sink for the analyte of interest overlain by a hydrogel diffusive layer for controlled diffusion from soil towards the BL.[15] This method has the potential to sample colloids from intact soils with minimal disturbance, provided that pore water colloids can freely diffuse into the DGT and bind to the BL. Colloids migrate to the BL by diffusion only, the method therefore neither disturbs the structure nor changes the local water flow. The DGT method also provides the opportunity to obtain spatially-resolved information on pore water colloid distributions in soils. DGT binding gels, analyzed with a spatially resolved method, like laser-ablation (LA) ICP-MS, have been able to provide high-resolution 2D images of the local diffusible solute in soils.[16] Applying the same approach to a colloid DGT could capture the heterogeneity of colloid concentrations in soils, reflecting variations caused by differences in water flow, chemical

attachment,[5] or small-scale processes driven by soil structure. Two studies previously developed DGT to sample small, engineered nanoparticles in soil and distinguished between truly dissolved ions and nanoparticles with duplicate DGT analysis, either with or without a dialysis membrane in front of the diffusive layer to regulate the passage of nanoparticles.[17,18] However, the method was neither ever used to sample pore water colloids, nor to visualise their distribution in intact soil to study microscale processes.

This study aimed to develop and demonstrate the concept of the DGT method to visualize pore water colloids in soil. A modified DGT setup is proposed with a thin membrane (9 µm), with large pore size (1 µm), and no diffusive gel layer to provide a short diffusion path for colloids. We recently identified a zirconium oxide-based BL, developed for oxyanions in DGT analysis, as the best-performing one for organomineral Fe colloids that were synthesized in the lab.[19] Since the technique employs a 1 µm filter, we refer in the manuscript to colloids rather than nanoparticles, although the latter constitute the most relevant and reactive mobile fraction. Here, the setup was tested for soil colloids with DGT deployed on intact soil cores at locations (*i.e.* soil and depths) where we expected high organo-mineral Fe colloid concentrations related to localised anaerobic microsites.[20] Spatially resolved analysis of the BL was done with synchrotron XFM and LA-TOF-ICP-MS aiming to identify colloidal P from co-localisation of Fe, Mn and P. On the same soil cores, pore water obtained by centrifugation was analysed by Field Flow Fractionation (FlFFF) to assist the DGT data interpretation. Colloid diffusion through the thin membrane and accumulation on the BL was later verified with soil colloid suspensions.

Material & methods

Field experiment and soil sampling

Six intact soil cores were sampled from the long-term QualiAgro field trial in Feucherolles (Yvelines, France), established in 1998 on a Glossic Luvisol (USDA soil classification) with silt loam texture. The trial assesses the agronomic and environmental effects of four organic amendments *versus* a control (CON). For this study, soils from CON, compost from municipal solid waste (MSW), and dairy farmyard manure (FYM) treatments were selected. This site was chosen based on previous findings of anaerobic microsites in the plough pan (28–35 cm depth), potentially acting as hotspots for colloidal P[20] and, therefore, the same field trial was revisited for new sampling. Long-term application of labile organic matter has been linked to increased reductive P mobilization and higher colloidal P concentrations in the plough pan compared to application with more stable organic amendments.[20] Most recent details on the field trial design,[21] which has evolved since 2013, and a soil profile description[22] is previously described. The topsoil (0–28 cm) pH was 7.0 for CON, 7.2 for MSW and 6.9

1936 | *Environ. Sci.: Nano*, 2026, **13**, 1935–1947

This journal is © The Royal Society of Chemistry 2026

for FYM, and the organic carbon content was 8.3 g OC per kg for CON and 11 g OC per kg for MSW and FYM. Oxalate-extractable concentrations were 20 mmol kg^{-1} Al (Alox), 50 mmol kg^{-1} Fe (Feox), and 7 mmol kg^{-1} Mn (Mnox). Near the plough pan, oxalate-extractable phosphorus (Pox) was 5.5 mmol kg^{-1} for CON, 7.6 mmol kg^{-1} for MSW and 10.0 mmol kg^{-1} for FYM.

The region has an average annual temperature of 10.8 °C and 647 mm of precipitation. Sampling followed an exceptionally wet winter: 233 mm of rain fell between Dec 1, 2023, and Feb 28, 2024. This is above the 90th percentile for this period (1950–present, Trappes station <10 km away; Section S1). On February 15, 2024, six intact soil cores (35 cm long, 5 cm diameter; two per treatment: CON, MSW, FYM) were sampled down to 45 cm depth after removing the top 10 cm, targeting the plough pan and slightly below. The soil cores were sampled with Plexiglas columns (5 cm inner diameter), cut in two halves along the longitudinal axis, both halves were held together with tape. A removable sharpened metal ring was attached to the bottom of the cores. The ring's inner diameter was 2 mm smaller than that of the columns to minimize soil compaction at the soil–column interface. A removable plastic holder was put on top of the columns to aid in their insertion into the soil, which was done by pushing and excavating the surrounding soil. A penetrometer confirmed the presence of the plough pan at each sampling point. Cores were stored at 4 °C and opened the next day for DGT deployment by carefully splitting them with a 0.1 mm stainless steel wire along the longitudinal axis to minimize vertical smearing. The DGT gels were deployed on these opened surfaces as described below.

Diffusive gradient in thin films-based method

The BL used in DGT analysis consisted of a polyacrylamide hydrogel mixed BL that combines micro-milled Chelex-100 resin,[23] which has paired iminodiacetate ions that strongly chelate polyvalent transition metal cations (targeting Mn^{2+} and Fe^{2+}), with *in situ* precipitated ZrO$_2$ targeting P sorption and organomineral Fe colloids.[24] First, the BL with micro-milled Chelex-100 resin was prepared.[23] The Chelex-100 resin was ground in an agate ball-mill (Retsch PM100, 30 min at 20 Hz) prior to gel preparation and a resin-water suspension was made at 10% w/v. To produce one gel, 1.25 mL resin suspension was mixed with 1 ml acrylamide (40%, Merck, Belgium) and 0.25 mL agarose-derivative crosslinker (2%, DGT Research Ltd, UK). Next, 17.5 μL ammonium persulfate (10%, Merck, Belgium) and 5 μL *N,N,N,N*-tetraethylenediamine (TEMED, Merck, Belgium) were added to the mixture. The gently mixed solution was cast between two glass plates assembled with a 250 μm-thick Teflon spacer to define the gel thickness. The assembly was placed in an oven at 45 °C for 1 h. The resultant gel was then put in ultrapure (UP) water (resistivity 18.2 MΩ, Milli-Q, EQ 7000, Merck) during one day for hydration with regular water replacement to remove residual synthesis byproducts. Next,

Zr was precipitated[24] in the Chelex gels. Gels are immersed for 3 hours in 0.1 M Zr solution, prepared from ZrOCl$_2$·8H$_2$O (2 gels in 100 mL) and ZrO$_2$ precipitation is accomplished by putting the gels in 0.1 M MES buffer at pH 6.7 for 40 min (2 gels in 40 mL). The gels were subsequently washed in UP water for 48 h with water replaced at least three times during this period. The gels were prepared to have a dimension (after hydration) of 16 cm in length, 5 cm in width and a thickness of 400 μm.

The diffusive layer in conventional DGT analysis consists of a protective membrane (150 μm thickness, 0.45 μm pore size) and a 800 μm thick hydrogel diffusive layer.[15] Here, only a 9 μm thin track-etched membrane filter with 1 μm pore size (ipPORE™, BE) was used to reduce the diffusion path for colloids. This membrane was selected to allow for sampling of colloids <1 μm. The track-etched membrane filter consisted of polycarbonate and is polyvinylpyrrolidone (PVP)-treated with pore density of 2 × 10^7 cm^{-2} and porosity of 15.7% (product ref: 1000M10/721M101/A4). A similar approach is often employed in high-resolution imaging DGT, where the hydrogel diffusive layer is replaced by a thin membrane (0.2 μm pore size, 10 μm thickness) separating soil and BL to minimize lateral diffusion and image blurring.[25]

The DGTs (16 cm length × 5 cm width) were deployed on soil cores to span the compacted plough pan and the underlying soil (25–41 cm depth), thereby excluding the upper 15 cm of the soil core. The location of the plough pan was around 28–35 cm depth and was visible on opened soil cores. Redoximorphic features were not visually detected in contrast with earlier findings.[20] Soils were slightly moistened with demineralised water immediately before gel deployment using a plant mister to ensure good soil–membrane contact. The stack of membrane, BL and a Perspex support was put in contact with one opened half soil core (one gel for each of the six cores). Both soil core halves (with and without DGT) were wrapped in cling film to avoid water loss, and the soil cores were stored in a 20 °C incubation room. A uniform weight of 12 kg (2 kg per soil core) was put on the soil core to maximise soil–DGT contact. The gels were removed from the soil after 24 h contact time and transferred, with the reactive side upwards, onto a membrane with 0.45 μm pore size (NC, Amersham Protran) supported by gel paper (Whatman). The gels were dried at room temperature in a vacuum drier (slab gel dryer, Hoefer Scientific Instruments, model SE1160) at room temperature for 6–9 hours with a clean PE sheet covering the reactive side. The dried gels were attached to a glass plate with double-sided tape, the reactive side facing upwards.

Binding layer imaging with X-ray fluorescence microscopy

The X-ray fluorescence mapping of Fe and Mn was performed at the XFM beamline of the Australian Synchrotron (ANSTO)

This journal is © The Royal Society of Chemistry 2026

Environ. Sci.: Nano, 2026, **13**, 1935–1947 | 1937

in Melbourne, Victoria. Both elements are indicative of redox hotspots and previously strongly correlated with soluble P[20]. They were therefore selected to screen the BL for smaller regions of interest to be analysed by LA-ICP-MS. Phosphorus was not measured with XFM because P analysis requires a specifically developed non-hydrogel-based BL to reduce self-absorption of the P fluorescence signal.[26] This BL was not used here as a mixed BL was required for combined metal and P detection with LA-ICP-MS. Samples were analyzed at the microprobe end-station with the Maia detector, details of the imaging settings are given in Section S2. Four BLs were analysed, one for CON (control where no Mn hotspots were expected) and FYM, and two for MSW as the first BL of this treatment did not reveal any regions of interest (ROI) of Mn.

Binding layer imaging with laser-ablation (LA) ICP-MS

A Teledyne Iridia excimer 193 nm laser-ablation system was coupled to TOFWERK ICP-TOF-R to analyse subsections (dimensions are given with the images) of the DGT BL based on the XFM maps. The cobalt cell and ARIS sample introduction was used for fast wash-out. The BL were ablated with a fluence of 1.5 J cm^{-2}, a square spot size of 20 μm and lines were scanned at 2000 μm s^{-1} and 50 Hz with interline spacing of 120 μm. The pixels were extrapolated laterally to provide a visual image where the pixel size was 40 × 120 μm. The *in situ*-precipitated ZrO_2 particles are typically ≤0.2 μm in size,[24] but the ground Chelex-100 resin beads remain considerably larger, up to ≤10 μm.[23] Furthermore, the nuclepore membrane used in the DGT assembly has 1 μm circular pores spaced approximately 1.24 μm apart. As a result, a 20 μm spot size was selected here, which is substantially larger than the size of individual colloids, enabling the detection of broader colloidal concentration zones rather than single particles. Redoximorphic features form in poorly drained soils due to Fe and Mn reduction under low oxygen conditions. These features appear as localized spots, or mottles, typically orange to grey, with medium-sized zones ranging from 6–20 mm.[27] Therefore, the 20 μm spot size (or 40 × 120 μm pixel size in the image) was deemed adequate for detecting redox hotspots. The ICP-TOF-MS allows full mass spectra analysis per extraction (functional minimum of ^{23}Na to ^{238}U). The ICP-TOF-MS measured spectra at a constant extraction rate of 33 kHz with one integrated spectrum produced for each laser shot by summing all material analysed within the washout period of the ablated material. This equated to an integration time of 16 ms for each laser shot, with one laser shot equating to one pixel in the final image. Daily operation included sensitivity maximisation and optimisation of single pulse response and extraction efficiency factor on the glass standard reference material NIST612. Gas blanks and NIST612 analysis were included at the start, middle and end of each sample for drift correction, which was generally negligible (<15%) for NIST612 after gas blank drift correction. Data was exported from TofDaQViewer to the LA

data processing software Iolite. Elemental maps (^{56}Fe, ^{27}Al, ^{28}Si, ^{55}Mn, ^{85}Rb, ^{133}Cs, ^{31}P, ^{44}Ca) were exported as text images and processed in ImageJ. Hotspots were identified following the procedure of Lehto *et al.* 2017,[28] with the modification that hotspots were defined as pixels exceeding the image-wide mean by 2 standard deviations. Hotspot identification was done with ImageJ and visualised in binary images.[28] The fractional overlap between hotspots of different elements was quantified using the JaCoP plugin to assess element co-localisation within the highest-intensity zones, thereby focusing on the most relevant areas rather than on low-concentration background signals.[29] Pixel-wise Pearson correlation coefficients (r) were calculated between elements for the entire images and for hotspots only. The pixel intensity values were log_{10}-transformed because that reduced skewness generally to values [−1,1]. The correlation analysis was performed in JMP® v17.

Pore water analysis

After DGT deployment, the soil pore water was extracted from the same soil core, for pore water analysis both halves of the soil core were used, while DGT was deployed only on one half. The soil sample was removed from the column, mixed and pore water isolated with a double chamber setup using centrifugation at 2000 g for 15 min (Thermo Multifuge X3R-swinging bucket). The pore water was subsequently fractionated at <0.45 μm to remove larger particles from the soil solution by means of additional centrifugation (10 min at 270 g). Fractionation with centrifugation is done instead of membrane filtration to reduce filtration artefacts.[10] To calculate centrifugation time for size fractionation of colloids, the particle density of phyllosilicates was used (2.5 g cm^{-3}). The pore water was analysed for dissolved organic carbon (DOC) with a TOC analyser (Shimadzu, TOC-L) and the elemental composition was measured by ICP-MS (Agilent 7700). The pore waters were analysed on the same day as the pore water extraction. A Tukey multiple comparison test was conducted to compare the mean elemental composition between groups using JMP® v17, with a significance level set at α = 0.05. The colloids in pore waters were characterised with field flow fractionation (FlFFF) (AF2000, Postnova Analytics) online coupled with a UV/vis detector (SPD-20A Postnova Analytics) and with ICP-MS with a previously described method,[30] further instrumental details are in Section S3. The UV/vis detector monitored the absorbance at wavelength 254 nm, which is commonly used in FlFFF analysis as a proxy for aromatic organic matter.[31] The ICP-MS monitored ^{31}P, ^{27}Al, ^{28}Si, ^{51}V, ^{55}Mn, ^{56}Fe, ^{65}Cu in time-resolved analysis. The ICP-MS calibration slopes were determined offline using multi-element certified standards acidified to 1% HNO_3. The median signal during focusing was subtracted from the signal during elution before multiplying with the calibration slopes to correct for the background signal. A moving average with interval 10 was calculated on the data to reduce signal noise. The

fractograms were divided into organic (retention time (T_r) 0–5 min) and mineral (T_r 5–82 min) colloid fractions, and colloidal concentrations were calculated by integration. These concentrations were expressed as fractions of the total pore water concentrations. Truly dissolved ions and small molecules (<1 kDa) are not measured with FlFFF analysis, therefore, their concentrations in pore water were estimated as the fraction of the total pore water concentration not recovered by FlFFF. The colloid composition is calculated at each time point from molar element ratios, and the median molar ratio over the relevant mineral colloid size range was taken.

Soil clay fractionation and characterisation

The pore water colloids were unexpectedly enriched in silicon (Si; see Results) and, therefore, clay colloids, rather than organomineral Fe colloids, became the focal point of this study. Clay minerals were extracted from soil to interpret the composition of colloids in FlFFF fractograms and to obtain a suspension to study colloidal clay uptake by DGT in controlled conditions (performance test, see below). The clay was obtained from the plough layer of MSW (75 g soil) and from FYM (25 g soil). Clay separation was done with a Jackson treatment[32] modified according to Zeelmaekers.[33] That method involved several chemical treatment steps to remove cementing agents (carbonates, organic matter and Fe/Al oxyhydroxides), details are given in Section S4. The remaining fraction was size-separated <0.2 μm and <2 μm by centrifugation. A subset of the <0.2 μm fraction (as a clay suspension) of MSW soil was used in the DGT performance test. For the remaining fractions (<0.2 μm and <2 μm of MSW and FYM) the clay mineralogy was determined by XRD analysis (Section S4) and the elemental composition of the clay was determined after digestion with the $LiBO_4$ fusion method in graphite crucibles[34] to break down the silicate structure and analysed by ICP-MS.

Performance test of DGT for suspensions of soil colloids and isolated clay

To test the binding of soil colloids on the BL, a performance test was set up. The test used i) native soil colloids extracted with 1 mM $CaCl_2$ from MSW soil and, in a separate test, ii) an isolated clay (<0.2 μm) suspension with pH 6.2, obtained using the Jackson treatment (see above). The Ca concentration in the extractant solution (1 mM $CaCl_2$) matched the Ca concentration in the pore water of the MSW soil (1.1 mM $CaCl_2$). Soil was incubated at 20 °C for two weeks at field capacity and extraction was done after 24 h end-over-end shaking in 12 pots containing 50 g soil with 0.25 kg L^{-1} solid–liquid ratio. The $CaCl_2$ extract was obtained after centrifugation for 10 min at 1365 g to obtain the size fraction ≤0.2 μm (calculated using Stokes' Law), the Al concentration in the extract was 294 μM. The clay suspension obtained after Jackson treatment contained about 10 g L^{-1} suspended clay, which was diluted in a 1 mM $CaCl_2$

background electrolyte to 20 μM Al. To quantify colloid sorption on the BL, the BLs were mounted in DGT pistons with the 1 μm nucleopore filter membranes (9 μm thickness) to separate the BL from the test solutions. Agarose gels of 1000 μm thickness were used as backing underneath the BL to fill up the DGT pistons to compensate for the thickness of the standard membrane (150 μm) and diffusive layer (800 μm). Nano-DGT[17] pistons were included to determine the truly dissolved fraction on the BL. They consisted of the nucleopore filter membrane, a 1 kDa dialysis membrane, the Chelex–Zr oxide BL, and an agarose backing hydrogel, and allow selective transport of truly dissolved ions to the BL. To verify that the BL acts as an effective binding phase (i.e. a zero-sink for colloids) rather than merely sampling colloids accumulating in the hydrogel, pistons without a binding phase were included. These were configured as DET (diffusive equilibrium in thin films) samplers and consisted of the nucleopore filter membrane, a polyacrylamide hydrogel (400 μm thickness) without Chelex resin or ZrO_2, and a 1000 μm polypropylene backing layer. In this configuration, colloids diffuse into the hydrogel without being irreversibly bound, providing a measure of colloid uptake in the gel alone. The thickness of DET hydrogels typically ranges from 800 to 1200 μm; here, a thinner hydrogel (400 μm) was used. This thickness matched that of the DGT BL, allowing direct comparison between clay colloid uptake on the BL and in the hydrogel alone to assess potential colloid sorption to the Zr oxide. Thicker hydrogels may not be fully penetrated by larger colloids and would require long equilibration times due to slow diffusion. There were 4 replicates per setup, hence in total 24 devices for both clay suspensions together. These devices were deployed for 48 h in stirred solutions (3 L soil extract or 3 L isolated clay suspension, 12 devices per 3 L). The suspensions were sampled initially and after 48 h, and the truly dissolved ion concentrations in the suspensions were sampled with dialysis (1 kDa cut-off), all samples were measured with ICP-MS. Three gel replicates were analysed by ICP-MS after microwave digestion at 210 °C in $H_2SO_4/HNO_3/HCl$ (details in Section S5). Detection of clay on the BLs after acid digestion was limited by low element recovery and dilution effects, therefore, a small subset of the gels (one DET and one BL replicate) from the performance test was analysed directly with LA-ICP-MS, thereby avoiding issues with extracting and dissolving the colloids in the gels. Each gel was analysed with 12 line scans, after gel drying following the procedure as described above. The LA-ICP-MS setup in this test was the Analyte Excite+ (Teledyne) and triple quadrupole ICP-MS (Agilent 8900), the settings are given in Section S6.

Results and discussion

Characterisation of pore water colloids obtained with centrifugation

The composition of the pore waters (<450 nm fraction) extracted from the plough layer and below (−20 to −45 cm

This journal is © The Royal Society of Chemistry 2026

Environ. Sci.: Nano, 2026, 13, 1935–1947 | 1939

Table 1 Composition of pore water samples (depth of 20–40 cm) obtained with centrifugation from 2 replicate cores per treatment: control without organic amendments (CON), municipal solid waste compost (MSW) and farmyard manure (FYM). Values are means ± standard deviation ($n = 2$), letters indicate statistically significant differences among treatments (all pairs Tukey HSD, $p < 0.05$)

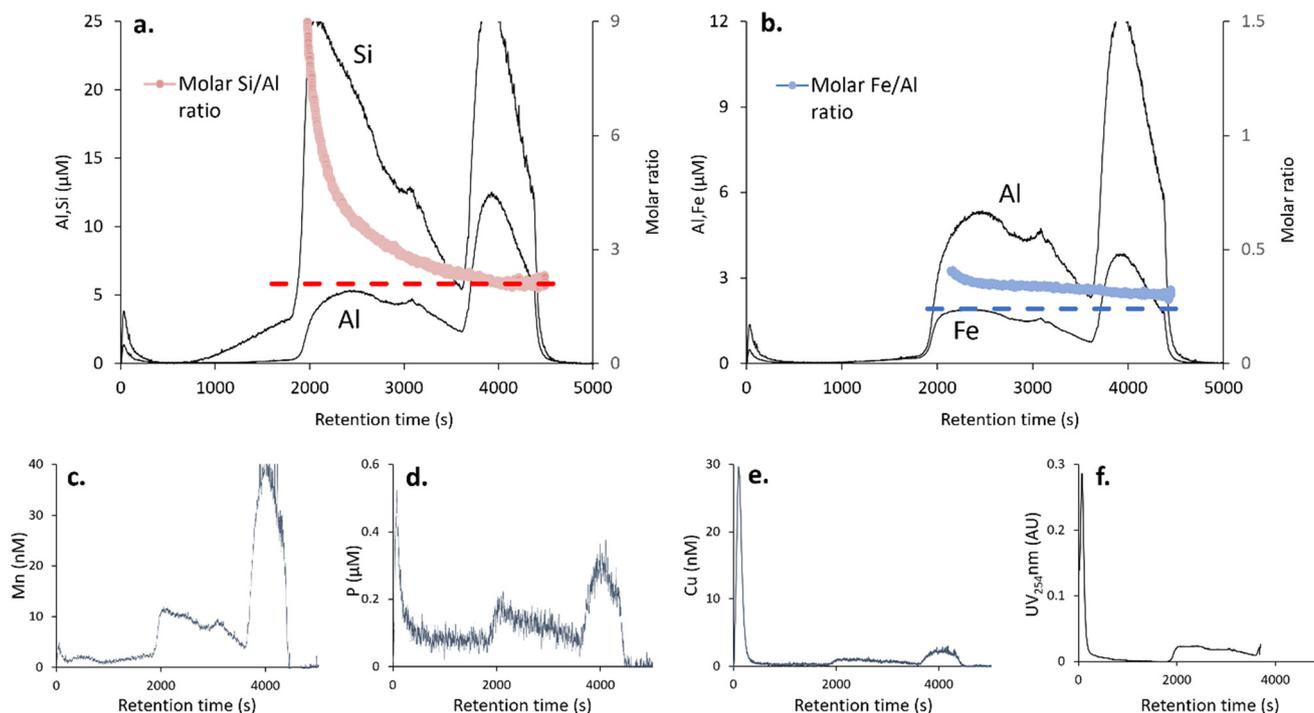|	DOC	Ca	Mg	P	Mn	Fe	Al	Si
	mM	mM	mM	μM	μM	μM	μM	μM
CON	1.19 ± 0.33	0.67 ± 0.02 (B)	0.08 ± <0.01 (B)	4.8 ± 0.4	0.40 ± 0.18 (B)	33 ± 13	86 ± 36	1063 ± 170
MSW	1.71 ± 0.18	1.12 ± 0.12 (A)	0.15 ± 0.03 (A, B)	5.0 ± 1.4	0.65 ± 0.04 (A, B)	45 ± 16	129 ± 40	1132 ± 18
FYM	2.42 ± 0.71	0.64 ± 0.06 (B)	0.19 ± 0.03 (A)	29.5 ± 16.3	1.07 ± 0.12 (A)	88 ± 23	242 ± 59	1246 ± 210

Fig. 1 FlFFF fractograms of the FYM pore water sample showing elemental signals (a–e) and the UV signal (f) as a function of colloid retention time (T_r), which corresponds to increasing colloid size. Organic colloids (<5 nm) elute at $T_r < 300$ s, while larger mineral colloids (5–450 nm) elute at $T_r > 300$ s. The red line in (a) shows the molar Si/Al ratio of the mineral colloids, the dotted red line indicates the Si/Al ratio of the clay fraction isolated from the soil. In the largest size fraction ($T_r > 3700$ s), the Si/Al ratio (2.1), matches that of the isolated clay. The blue line in (b) shows the molar Fe/Al ratio of the mineral colloids, the dotted blue line the ratio of the isolated clay. The Fe/Al ratio in the mineral colloids is only slightly higher than in the isolated clay.

depth) of the 6 intact soil cores is given in Table 1. The Fe, Al and Mn are given because oxides of these elements are the dominant mineral colloids that bind P. In all pore waters, concentrations of Al are considerably higher than those of Fe and Mn.

The pore water colloid characterisation with FlFFF is presented for the FYM soil. Fig. 1 shows the concentrations of several elements, including Si, Al, Fe and the UV absorbance, as a function of elution time. The results show a high UV peak at low retention times ($T_r < 300$ s), which corresponds with a particle size of approximately 1–5 nm. This peak with high UV absorbance at small size is attributed to humic substances in the pore water, which occur in this size range and have a high UV absorbance at 254 nm due to aromaticity.[31] In addition, Cu, which has a high affinity

for humic substances also closely follows the UV signal (Fig. 1). Conversion of the UV absorbance to an organic carbon (OC) concentration using the Specific UV absorbance (SUVA) of fulvic acids (after correction for Fe (ref. 30)) indicates that OC is the mean constituent in that size fraction (peak of 0.68 mM OC, Fig. 1). The Fe and Al in this size fraction correspond with complexes with organic matter, but the contribution of these forms to their total pore water concentrations is small (<1% of total pore water concentration in FYM soil, <2% in MSW and CON soil, Section S7). The higher retention times in the FlFFF fractogram ($T_r > 300$ s) correspond to larger mineral colloids. For the second and third elution peak in the fractogram at longer retention time (larger size: 5–450 nm), Si is the main constituent, followed by Al, and Fe, while Mn is a minor component (Fig. 1). The Si/Al ratio

in the larger mineral colloids of the FYM soil ($T_r > 3600$ s) equals 2.1, which is characteristic for 2:1 phyllosilicates. Clay colloids have previously been identified using FlFFF analysis.[35]

To interpret the composition of the mineral pore water colloids, given the dominance of clay colloids, the clay mineralogy and composition in soil was determined after clay isolation by the Jackson treatment.[32] The XRD analysis indicated that the clay fraction with particle size <0.2 μm primarily consists of the 2:1 clay types illite, smectite, mixed layer illite–smectite and the 1:1 type clay kaolinite (Fig. 2 and Section S8). Digestion indicated that the clays have structural Fe, the molar Fe/Al ratio in the isolated <0.2 μm clay fractions is 0.24 (Fig. 2). This is only slightly lower than the molar ratio in the mineral pore water colloids of the three soils measured in the FlFFF fractograms (0.33–0.34). Note that the clay isolation method with the Jackson treatment included removal of Fe oxides with citrate–bicarbonate–dithionite (Section S4). This suggests that the Fe in pore water colloids is largely structural Fe within the clay colloids, while to a lesser extent Fe in the colloids could be sorbed or precipitated on clays as hydrolysed Fe species.[36] It is remarkable that the colloids with molar Fe/Al 0.33 are found consistently in the pore waters of the three soils (Section S7) and also in the $CaCl_2$ extracts of the previous study.[20] A plot of Fe *versus* Al in the $CaCl_2$ extracts yielded a slope of 0.34 mol Fe per mol Al ($r^2 = 0.75$), which indicates a mobile colloidal fraction with characteristic composition. The pore waters of the three soils likely also contain small SiO_2 nanoparticles, concluded from the Si peak at T_r 2000 s (size 100 nm), and no other elements following the same size distribution of Si (Fig. 1). The fractograms of the two other soils, MSW and CON soil are given in Section S7 and show similar results as the FYM soil.

We previously identified high DOC and low Ca concentrations as primary factors explaining the presence of organomineral Fe oxide colloids in soil pore waters.[30] In soils with high organic carbon (OC), small organo-mineral Fe oxide colloids dominated, whereas in low-OC soils, larger clay colloids associated with Fe oxides were more prevalent. In the deeper layers of this Luvisol, DOC concentrations are likely too low to stabilise organo-mineral Fe colloids. In addition, the low pore water Ca levels (<1.20 mM) favour clay dispersion.[37] As a result, clay colloids seem to dominate over organo-mineral Fe oxide colloids in these pore waters. This observation is also consistent with the typical characteristics of Luvisols, where the presence of a Bt horizon indicates the accumulation of translocated clay.

The FYM soil had the highest pore water P concentration (Table 1). FlFFF analysis shows that pore water P in FYM occurs mainly as truly dissolved species (77%), with smaller contributions from organic P (3.3%) and mineral colloid-associated P (19%) (Section S7). In contrast, soils with lower pore water P contained a larger colloidal P fraction (70% in MSW and 53% in CON), likely due to colloid saturation at high P concentrations in the FYM soil.[20] Although P co-eluted with mineral colloids in the FlFFF analysis, binding is weak (molar P/(Fe + Al) = 0.021), substantially lower than P binding to amorphous oxides at the same depth ($P_{ox}/(Fe_{ox} + Al_{ox})$ = 0.13), also suggesting that only a fraction of colloidal Fe and Al occurs as oxides. In an anaerobic incubation experiment with soil samples taken near the plough pan of this soil,[20] Mn reductive dissolution induced colloidal P in the soils amended with labile organic matter (FYM and MSW), but this process was observed at much higher Mn concentrations (*i.e.* more reduced conditions) than we found in the field. In all soils, the Mn concentration was at least an order of magnitude lower than P, indicating that reductive Mn dissolution was not a
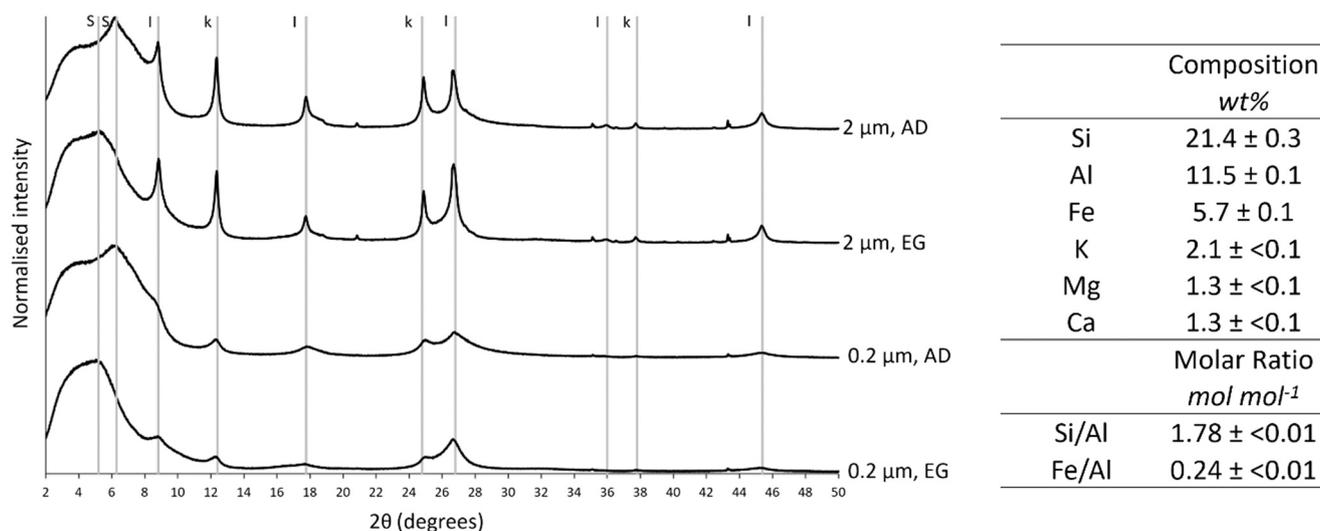

	Composition
	wt%
Si	21.4 ± 0.3
Al	11.5 ± 0.1
Fe	5.7 ± 0.1
K	2.1 ± <0.1
Mg	1.3 ± <0.1
Ca	1.3 ± <0.1
	Molar Ratio
	mol mol^{-1}
Si/Al	1.78 ± <0.01
Fe/Al	0.24 ± <0.01

Fig. 2 XRD patterns of clay fractions (<2 μm & <0.2 μm) isolated from MSW soil, both air-dried (AD) and with ethylene glycol (EG) treatment to identify expandable clays. The clay composition analysis is for the fraction <0.2 μm.

This journal is © The Royal Society of Chemistry 2026

Environ. Sci.: Nano, 2026, **13**, 1935–1947 | 1941

dominant mechanism to explain pore water P at this sampling event.

Visualisation of pore water colloids with DGT

Soil structural heterogeneity previously promoted the formation of localized anaerobic microsites and associated hotspots of colloidal P[20], which motivated the use of intact soil samples in this study. Such hotspots occurred in the plough pan of this loamy soil that was otherwise well-drained; the combination of higher soil bulk density with low pH and high organic matter content in the plough pan previously led to these conditions.[20] The XFM analysis was used to screen the entire DGT BL for the redox-sensitive elements Fe and Mn, smaller regions of interest were subsequently analysed with LA-TOF-ICP-MS that detects almost the full mass range with high sensitivity. The LA-ICP-MS and XFM detected similar features for Fe on the same BL, but the XFM had lower sensitivity for Mn (Section S9). Only in the BL of FYM, locally high Mn zones were detected with XFM, two areas at the top of the plough pan of approximately 2.0 cm^2 and 1.7 cm^2 and a few smaller spots at greater depth. The LA-ICP-MS also detected these areas as zones with high Mn, but also detected Mn at lower concentrations in all samples, which is discussed first.

A selection of elemental maps from MSW soil obtained with LA-ICP-MS is given in Fig. 3. The spatial distribution of Fe, Si, Al and Mn, the main elements in mineral colloids, was very similar, which suggests the presence of oxide-clay colloids, as observed in the pore water analysis (Fig. 1). Element co-localisation was calculated from pixel-wise correlation coefficients (r) on the entire image, which was ≥ 0.96 between Al and Fe (Fig. 4) and between Al, Si and Mn in MSW soil (Section S10). The presence of clay colloids would imply the colocalization of other major elements of clay minerals (*i.e.* K, Mg, Ca), which is indeed confirmed by strong pairwise correlations. The pairwise correlation

coefficients between all these elements is at least 0.97, except for Ca where the correlation coefficients are lower ($r \geq 0.58$), which is further discussed below. In addition, owing to the non-target analysis of the TOF-ICP-MS, rubidium (Rb) and caesium (Cs) maps were also recorded (Fig. 3). Remarkably strong correlations ($r \geq 0.94$) were also found between Al and Rb (Fig. 4) and Cs, which are the most convincing correlations indicative of clay colloids. The Rb and Cs are tracers of 2 : 1 type clay minerals because these alkali metal cations selectively bind to the frayed edges of weathered mica's to balance the negative charge resulting from isomorphic substitution.[38] Hotspot analysis in the elemental maps show a high degree of spatial overlap among these elements ($\geq 83\%$), indicating that the highest intensity areas of Al, Fe, Si, Mn, Rb and Cs predominantly occur together. This high co-occurrence indicates a limited presence of other Fe and Al species, *i.e.* DOC complexes and truly dissolved ions, in line with the FlFFF results. Pixel-wise correlation coefficients and hotspot analysis of the two other soils show very similar results, the data are given in Section S10 and S11. The *in situ* deployed DGT method thus allowed the detection of pore water clay colloids when present in pore water at concentrations of 20 mg clay per L (calculated from the Al concentration in CON soil and the composition of the clay).

Spatial distribution of pore water colloids in intact soil

The colloid distribution on the BL is spatially heterogeneous (Fig. 3), this likely reflects areas of higher and lower colloid abundance rather than artefacts caused by poor membrane-soil contact. This is supported by the observation that background regions for colloids still contain other elements (*e.g.* P, Ca Fig. 3). It is remarkable that despite Ca being part of the clay mineral structure, the correlation between Al and Ca was not strong (r 0.60, in contrast to Al with Mg, r 0.99) and not well-described by a linear relation as shown in Fig. 4.
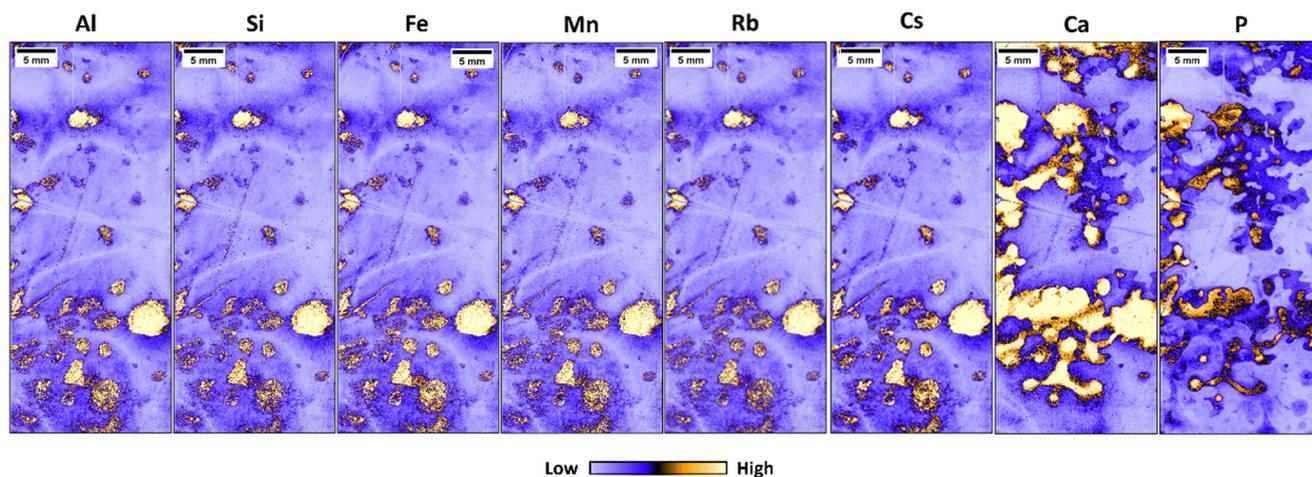

Fig. 3 Elemental maps of the BL deployed on the plough pan of soil amended with municipal solid waste (MSW), the colour scale indicates low to high intensity values. The size of the image is 21 × 52 mm.
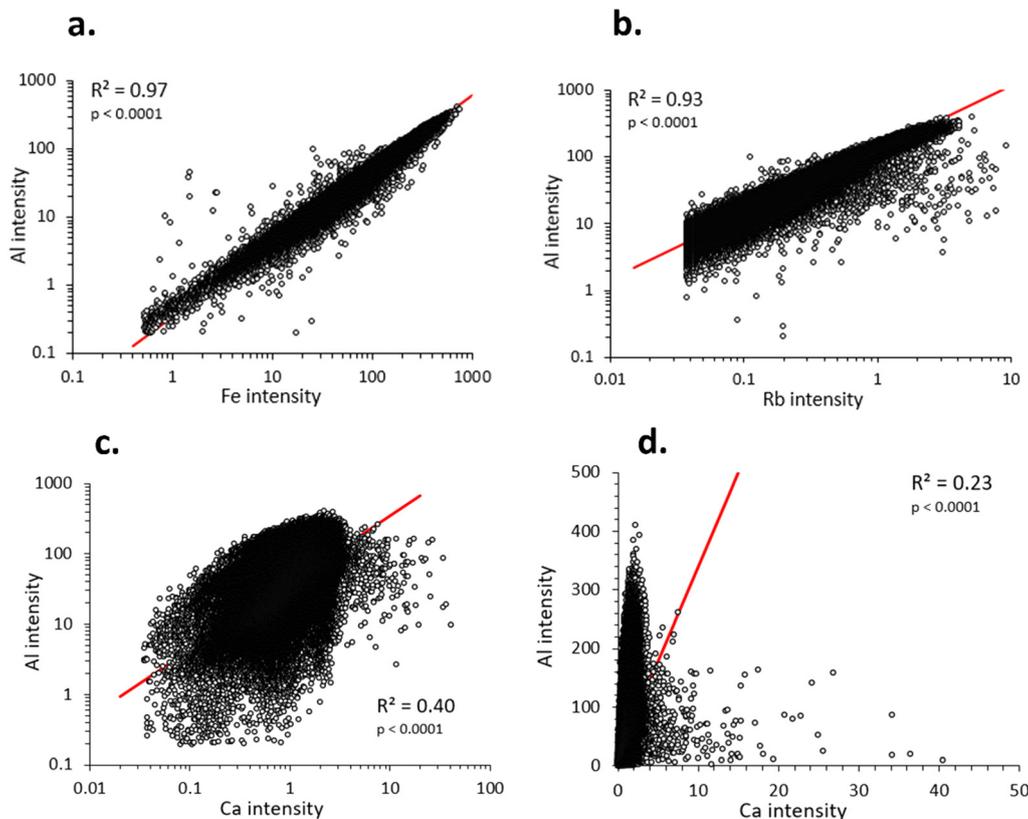
1942 | *Environ. Sci.: Nano*, 2026, **13**, 1935–1947

This journal is © The Royal Society of Chemistry 2026

Fig. 4 Correlation analysis of the full MSW soil image indicates strong pixel-wise correlations on log-transformed data between Al and Fe (in a) and between Al and Rb (in b). Rubidium, which preferentially binds to frayed-edge sites of 2 : 1 clay minerals, serves as a tracer for these minerals. In contrast, the correlation between Al and Ca (in c) is weak, because Ca on the BL is dominated by truly dissolved Ca with only a minor contribution from clay-bound Ca. The untransformed correlation data between Al and Ca (in d) further shows that the highest Al intensities occur at low Ca intensities, consistent with enhanced dispersion of clay colloids under low-Ca conditions.

The Ca in pore water is mainly ionic, the clay-derived Ca in the pore water is 1% of the total (calculated from the composition of clay and with the clay concentration calculated from pore water Al, see above), therefore, the Ca

on the BL mostly represents truly dissolved Ca. This is different for Mg that has lower pore water concentration than Ca (Table 1) and higher concentration in the clay (Fig. 2). Elemental maps show that clay colloids are absent from
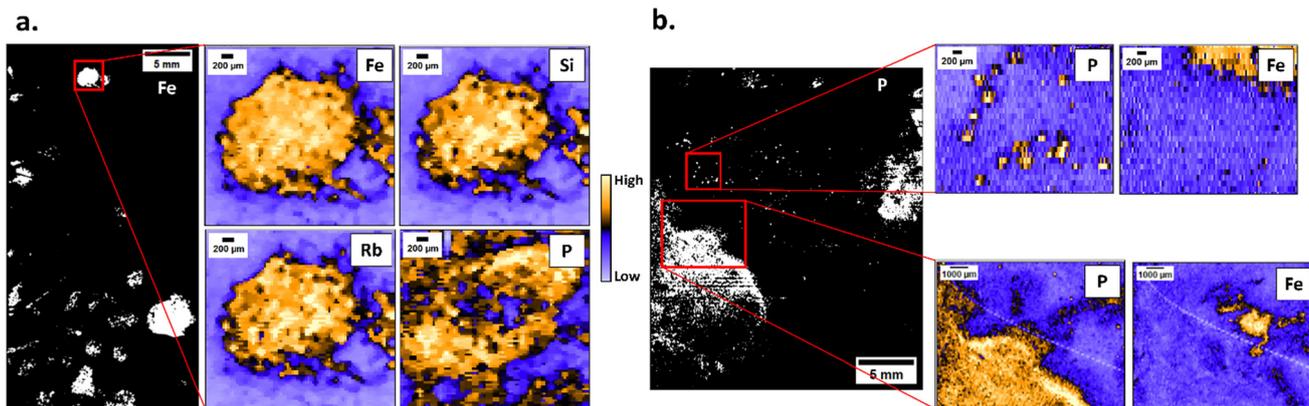

Fig. 5 Hotspot analysis on the BL of MSW soil (a) and FYM soil (b). Binary maps of *Fe hotspots* (white; background black) are shown (in a) with corresponding zoomed-in maps of Fe, Si, Rb, and P. The Fe, Si, Rb maps show overlapping hotspot areas, where P is also locally enriched but shows a distinct spatial distribution. Of note is that only colloids smaller than the membrane pore size (1 μm) could diffuse towards the BL, the hotspots therefore represent zones of elevated colloid concentrations, not individual colloids. Binary map of *P hotspots* (in b) with corresponding zoomed-in maps of P and Fe in two areas further indicates limited colocalization with Fe, suggesting that a substantial fraction of P is not Fe-associated colloidal P in this soil with the highest pore water P. The colour scale indicates low to high intensity values.

regions with the highest Ca concentrations (Fig. 4), consistent with the known effect of low Ca levels promoting clay dispersion. We hypothesise that the location of clay colloids on the BL may correspond with areas in soil with larger pores and higher water flow, leading to shorter residence times and lower Ca concentrations. In contrast, zones with elevated Ca may reflect smaller pores with reduced flow and longer residence times. The low correlation between Al and Ca is consistently observed also in FYM (r = 0.64) and CON soil (r = 0.25), Section S10.

Co-localisation of P with colloids on the BL

Fe and P colocalised in some areas (Fig. 3), but there is no strong linear relationship between P and Fe on the whole image in the MSW soil (r = 0.49). With increasing Fe, also P increased locally, but the highest P occurred in regions where Fe was relatively low (Section S10). We further examined whether correlations between Fe and P improved when analysis was restricted to Fe hotspots. However, correlations between P and Fe, as well as between P and Fe/Si (indicative of Fe-enriched clay colloids), remained very weak ($r \leq 0.13$, Section 11). In addition, the overlap between P hotspots and Fe hotspots was low, 18% of P hotspots co-occurred with Fe hotspots. This is shown for instance in Fig. 5, with a zoomed-in view of one of the Fe hotspots in MSW soil. The Fe, Si, Rb maps show overlapping hotspot areas, where P is also locally enriched but shows a distinct spatial distribution. This analysis suggests that colloids contribute little to pore water P, which appears inconsistent with the FlFFF results, that showed that a substantial fraction (70%) of pore water P in this soil is colloid-associated (see above). While factors such as *in situ* DGT sampling *versus* disturbed sampling with centrifugation may contribute to differences, the apparent discrepancy likely also arises because mineral colloids, truly dissolved and organic P all contribute differently to DGT fluxes. Colloids diffuse more slowly than ions, and their resupply from the solid phase is uncertain, therefore, their flux to the DGT is likely limited, leading to an enrichment of truly dissolved P at the binding layer relative to colloids compared with the pore water composition. Quantifying colloidal P using DGT requires back-calculation of solute and colloid fluxes to resident pore water concentrations, more advanced modelling is required to reconstruct resident pore water composition for different species from 2D DGT images. The element most strongly correlating with P in all samples is Ca (for instance r = 0.80 in MSW soil), which might be because both were predominantly truly dissolved in the pore water, and therefore do not follow the colloidal distribution.

Fig. 5 shows P hotspots in FYM soil with corresponding zoomed-in map of P and Fe, showing the absence of Fe at high P in this soil with the highest pore water P. Only in this BL deployed on FYM soil, local high Mn concentrations were found in two areas (Section S9). These zones with high Mn did not correlate with Si, Al, Fe (and other elements related to clay). It is, therefore, possibly truly dissolved Mn due to

reductive dissolution in the compacted plough pan as previously described for this easily-degradable organic matter amendment.[20] Although P co-localised with Mn, P was not strongly increased locally where that high Mn was found. The Mn dissolution may be too low to increase P beyond the truly dissolved P concentration as the FYM soil already had relatively high truly dissolved P near the plough pan (Table 1). Previous work also showed that reductive dissolution of Mn only markedly increased P at dissolved Mn concentrations higher than 100 μM,[20] *i.e.*, concentrations two orders of magnitude higher than in the pore waters sampled here. While this DGT method was developed to visualise local colloid and solute concentrations at sub-mm scale, we could not observe the anticipated colloidal P release mechanism in anaerobic microsites[20] (*i.e.* absence of strong co-localisation between Fe, Mn and P) in the compacted plough pan during this sampling campaign.

Performance test of DGT for suspensions of soil colloids and pure clay

The Zr-based BL has previously been shown to bind organomineral Fe colloids.[19] Since clay sorption was never verified, an *a posteriori* validation experiment with two clay suspensions was set up to investigate clay binding on the BL. Acid digestion of clay on BLs resulted in poor recovery of colloidal Al and Si, while Cs, Rb remained below detection limits. There was good recovery of Fe, but sorption from the isolated clay suspension, which had lower clay concentration than the soil extract, was largely below detection limits (Section S12). For the soil extract, the BL in DGT accumulated 8.88 ± 2.14 nmol Fe per cm^2, while the nano-DGT accumulated 4.38 ± 1.53 nmol Fe per cm^2. Subtracting the nano-DGT contribution yielded a colloidal Fe loading of 4.5 nmol Fe per cm^2 on the BL, neglecting the slight increase in diffusive layer thickness for the nano-DGT compared to DGT due to the dialysis membrane. This corresponds to approximately 4.44 ± 2.63 μg of clay per cm^2 for the soil extract and confirms that the BL binds clay colloids in addition to dissolved ions. LA-ICP-MS line-scan data further demonstrated enhanced accumulation on the DGT BL compared to DET, indicating sorption to the binding phase rather than simple colloid entrapment in the hydrogel. This was evident for Al (Fig. 6) and similarly observed for Fe, Si, and Rb (Section S12). However, because ions diffuse faster than colloids and may sorb selectively to the BL (*e.g.* Al^{3+} to Chelex), part of the elemental signal on the BL likely represents truly dissolved species. Therefore, an estimate of the colloidal fraction and truly dissolved fraction on the DGT BL and DET was made based on Al as an example. Truly dissolved Al on the BL was estimated using the DGT equation and dialysis concentrations (Section S12), yielding 1.56 nmol Al per cm^2 for the isolated clay suspension and 29.7 nmol Al per cm^2 for the soil extract (light grey bars in Fig. 6). The LA-ICP-MS data were not calibrated, therefore, the total mass loading of Al on the DET was estimated assuming
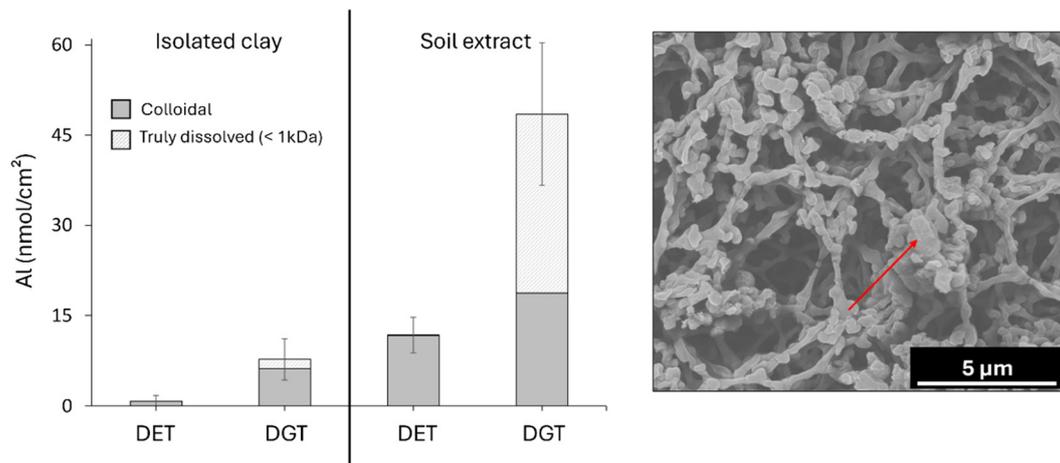
1944 | *Environ. Sci.: Nano*, 2026, **13**, 1935–1947

This journal is © The Royal Society of Chemistry 2026

Fig. 6 Left: Al accumulation on hydrogels with Zr–Chelex (referred to as DGT) and without (referred to as DET) for devices deployed in an isolated clay suspension and in a 1 mM CaCl$_2$ soil extract. Values represent means ± standard deviation from LA-ICP-MS line scans on 1 gel replicate. The BL was able to accumulate clay colloids because Al is higher in DGT *versus* corresponding DET samples. The truly dissolved Al contribution for DET and DGT is indicated and was estimated based on suspension composition and deployment time (details in Section S12). Right: SEM image of the dried BL after deployment in the isolated clay suspension (<0.2 μm fraction), the red arrow points to retained clay colloids in the gel matrix.

equilibrium with the suspension; for the DGT BL it was estimated from the counts of Al on the BL based on a two-point calibration using both DET data. The total estimated BL concentration in DGT is 7.7 nmol per cm^2 for the isolated clay and 48 nmol per cm^2 for the soil extract (Fig. 6, total height of bar graphs). These estimates indicate that Al accumulated on the BL in the isolated clay suspension was predominantly colloidal (6.1 nmol Al per cm^2), which is an eightfold increase compared to DET (0.796 nmol colloidal Al per cm^2, also corrected for truly dissolved Al, Fig. 6). For the soil extract, colloidal Al on the DGT BL (18.8 nmol Al per cm^2) was approximately twice that in DET (11.7 nmol Al per cm^2), suggesting enhanced binding to the BL, although saturation of the Chelex–Zr oxide binding phase may have occurred. The colloidal Al loading on the DGT BL of the soil extract of 18.8 nmol Al per cm^2 corresponds to approximately 4.41 μg of clay per cm^2 based on the clay stoichiometry, this is in good agreement with the nano-DGT-derived clay binding from the soil extract.

Scanning electron microscopy (SEM) analysis on the dried BL deployed in the isolated clay suspensions (<0.2 μm fraction) confirmed the presence of clay colloids in the gel matrix (Fig. 6, right panel). The mechanism of clay sorption on the Chelex–Zr oxide BL might be due to cation bridging. Multivalent cations (*e.g.* Ca^{2+} in soil solution and isolated clay suspension) might act as a bridge between the negatively charged clay colloid and the negatively charged zirconium oxide surface, which has a point of zero charge <4 at 25 °C in background electrolyte of ≤0.1 M NaNO$_3$.[39] In further experiments, the linear range of colloid uptake (in comparison to DET or nano-DGT at equal points) on the BL *versus* time and *versus* increasing colloidal concentrations still has to be determined.

The 2:1 phyllosilicate clays, such as illite, predominantly have a permanent surface charge and are therefore expected to retain a net negative surface charge across the agronomically relevant pH range (~5–8), making substantial losses in uptake on the DGT BL unlikely under typical conditions. Sampling may be affected for clay colloids with predominantly pH-dependent surface charge. Metal oxide colloids associated with organic matter in pore waters, and organic matter itself, also have pH-dependent surface charge. However, the Zr oxide binding layer was specifically developed to sample such colloids, with binding governed not solely by electrostatic interactions, but predominantly through complexation *via* functional groups of the NOM on the Zr oxide.[19]

Conclusion

Taken together, we developed a DGT-based method to sample pore water colloids *in situ* in soil to improve the prediction of colloid-facilitated transport of nutrients and contaminants. Our study illustrates that the low sensitivity of the standard DGT method towards colloids, due to their slow diffusion through the diffusive hydrogel layer,[40] can be overcome with a colloid-accumulating BL in combination with a thin membrane (9 μm) diffusive layer. The application in intact soil cores showed that, under the conditions and in the soils examined here, the colloids were mainly clay colloids, as evidenced by elemental co-localisation in image analysis. This might not be surprising given that samples were taken in the eluviated A2 horizon of a Luvisol after a high winter rainfall. The nature of the colloids on the BL matched those found in the pore water samples taken on the same soil cores and analysed with FlFFF, which corroborates the DGT findings. This study focused on high-resolution visualisation of pore water colloids in soil to explore the possibility of detecting small-scale colloidal processes (sub mm-scale) that arise from soil structural heterogeneity. Such *in situ* sampling

can reduce artefacts associated with pore water extraction methods and uniquely provides spatially resolved, two-dimensional information on colloid distribution. Of note is that the identification of clay minerals in the spatially resolved DGT analyses is currently still insufficiently quantitative. Firstly, the LA-ICP-MS data are not calibrated to matrix-matched standards with clay minerals accumulated on the gel. Secondly, the concentration of the clays on the DGT in the model suspensions suggests that the DGTs act as clay sinks and this requires more complicated modelling to convert that to meaningful *in situ* pore water concentrations; the standard principles derived for solutes[41] are unlikely to work for pore water colloids. In addition, further validation across soils with contrasting pH ranges and colloid composition is required to fully constrain the applicability for soil colloids. Nevertheless, our results demonstrate that *in situ* DGT mapping, using the DGT developed for colloids, offers new opportunities to better understand colloid-related processes in soil.

Conflicts of interest

All authors declare that they have no competing financial interests or personal relationships that could have influenced the work reported in this paper.

Data availability

The research data will be made available upon reasonable request.

Supplementary information (SI) is available. See DOI: https://doi.org/10.1039/d5en01069a.

Acknowledgements

References

1   K. Totsche, W. Amelung, M. H. Gerzabek, G. Guggenberger, E. Klumpp, C. Knief, E. Lehndorff, R. Mikutta, S. Peth, A. Prechtel, N. Ray and I. Kögel-Knabner, Microaggregates in soils, *J. Plant Nutr. Soil Sci.*, 2018, **181**, 104–136.

2   B. D. Kay, Rates of Change of Soil Structure Under Different Cropping Systems, in *Advances in Soil Science 12. Advances in Soil Science*, ed. B. A. Stewart, Springer, New York, NY, 1990, vol. 12.

3   M. Hassellöv and F. von der Kammer, Iron Oxides as Geochemical Nanovectors for Metal Transport in Soil-River Systems, *Elements*, 2008, **4**(6), 401–406.

4   B. Bergen, J. Lemmens, C. Moens and E. Smolders, Colloids facilitate transport of cadmium and uranium in arable soils which is undetected by suction cups in the field, *Eur. J. Soil Sci.*, 2024, **75**(2), e13480.

5   R. Kretzschmar, M. Borkovec, D. Grolimund and M. Elimelech, Mobile Subsurface Colloids and Their Role in Contaminant Transport, *Adv. Agron.*, 1999, **66**(C), 121–193.

6   R. Warrinnier, T. Goossens, F. Amery, T. Vanden Nest, M. Verbeeck and E. Smolders, Investigation on the Control of Phosphate Leaching by Sorption and Colloidal Transport : Column Studies and Multi-Surface Complexation Modelling, *Appl. Geochem.*, 2019, **100**, 371–379.

7   I. C. Regelink, G. F. Koopmans, C. van der Salm, L. Weng and W. H. van Riemsdijk, Characterization of Colloidal Phosphorus Species in Drainage Waters from a Clay Soil Using Asymmetric Flow Field-Flow Fractionation, *J. Environ. Qual.*, 2013, **42**, 464.

8   J. Siemens, K. Ilg, F. Lang and M. Kaupenjohann, Adsorption Controls Mobilization of Colloids and Leaching of Dissolved Phosphorus, *Eurasian J. Soil Sci.*, 2004, **55**, 253–263.

9   S. Beauchemin, R. R. Simard and D. Cluis, Forms and Concentration of Phosphorus in Drainage Water of Twenty-Seven Tile-Drained Soils, *J. Environ. Qual.*, 1998, **27**, 721.

10 C. Moens, N. Waegeneers, A. Fritzsche, P. Nobels and E. Smolders, A systematic evaluation of Flow Field Flow Fractionation and single-particle ICP-MS to obtain the size distribution of organo-mineral iron oxyhydroxide colloids, *J. Chromatogr. A*, 2019, **1599**, 203–214.

11 C. E. Geibe, R. Danielsson, P. A. W. van Hees and U. S. Lundström, Comparison of soil solution chemistry sampled by centrifugation, two types of suction lysimeters and zero-tension lysimeters, *Appl. Geochem.*, 2006, **21**, 2096–2111.

12 K. Ilg, E. Ferber, H. Stoffregen, A. Winkler, A. Pekdeger, M. Kaupenjohann and J. Siemens, Comparing Unsaturated Colloid Transport through Columns with Differing Sampling Systems, *Soil Sci. Soc. Am. J.*, 2007, **71**(2), 298–305.

13 J. M. Shira, B. C. Williams, M. Flury, S. Czigány and M. Tuller, Sampling Silica and Ferrihydrite Colloids with Fiberglass Wicks under Unsaturated Conditions, *J. Environ. Qual.*, 2006, **35**, 1127–1134.

14 B. Nowack, S. Koehler and R. Schulin, Use of Diffusive Gradients in Thin Films (DGT) in Undisturbed Field Soils, *Environ. Sci. Technol.*, 2004, **38**, 4.

15 W. Davison and H. Zhang, Progress in understanding the use of diffusive gradients in thin films (DGT) – back to basics, *Environ. Chem.*, 2012, **9**, 1–13.

16 J. Santner, T. Prohaska, J. Luo and H. Zhang, Ferrihydrite Containing Gel for Chemical Imaging of Labile Phosphate Species in Sediments and Soils Using Diffusive Gradients in Thin Films, *Anal. Chem.*, 2010, **82**, 7668–7674.

17 H. M. Pouran, F. L. Martin and H. Zhang, Measurement of ZnO nanoparticles using diffusive gradients in thin films: binding and diffusional characteristics, *Anal. Chem.*, 2014, **86**, 5906–5913.

18 R. Sekine, G. Brunetti, E. Donner, M. Khaksar, K. Vasilev, A. Jämting, K. Scheckel, P. Kappen, H. Zhang and E. Lombi, Speciation and Lability of Ag-, AgCl- and Ag$_2$S-Nanoparticles in Soil Determined by X-ray Absorption Spectroscopy and Diffusive Gradients in Thin Films, *Environ. Sci. Technol.*, 2015, **49**, 897–905.

19 J. Ceulemans, C. Moens and E. Smolders, Binding gel optimisation for the detection of organomineral iron colloids with the Diffusive Gradients in Thin films method, *Anal. Chem.*, 2025, **97**, 26384–26392.

20 R. Warrinnier, S. Bossuyt, C. Resseguier, P. Cambier, S. Houot, J. P. Gustafsson, J. Diels and E. Smolders, Anaerobic Respiration in the Unsaturated Zone of Agricultural Soil Mobilizes Phosphorus and Manganese, *Environ. Sci. Technol.*, 2020, **54**(8), 4922–4931.

21 H. Chen, F. Levavasseur and S. Houot, Substitution of mineral N fertilizers with organic wastes in two long-term field experiments: Dynamics and drivers of crop yields, *Soil Use Manage.*, 2024, **40**, e13079.

22 P. Cambier, V. Pot, V. Mercier, A. Michaud, P. Benoit, A. Revallier and S. Houot, Impact of Long-Term Organic Residue Recycling in Agriculture on Soil Solution Composition and Trace Metal Leaching in Soils, *Sci. Total Environ.*, 2014, **499**, 560–573.

23 C. Zhou, S. van de Velde, W. Baeyens and Y. Gao, Comparison of Chelex based resins in diffusive gradients in thin-film for high resolution assessment of metals, *Talanta*, 2018, **186**, 397–405.

24 D. X. Guan, P. N. Williams, J. Luo, J. L. Zheng, H. C. Xu, C. Cai and L. Q. Ma, Novel Precipitated Zirconia-Based DGT Technique for High-Resolution Imaging of Oxyanions in Waters and Sediments, *Environ. Sci. Technol.*, 2015, **49**(6), 3653–3661.

25 J. Santner, M. Larsen, A. Kreuzeder and R. N. Glud, Two decades of chemical imaging of solutes in sediments and soils – a review, *Anal. Chim. Acta*, 2015, **878**, 9–42.

26 C. Moens, E. Lombi, D. Howard, S. Wagner, J. L. Payne, P. M. Kopittke and C. L. Doolette, Mapping Phosphorus Availability in Soil at a Large Scale and High Resolution Using Novel Diffusive Gradients in Thin Films Designed for X-ray Fluorescence Microscopy, *Environ. Sci. Technol.*, 2024, **58**(1), 440–448.

27 Food and Agriculture Organization of the United Nations (FAO), *Guidelines for soil description*, Food and Agriculture Organization of the United Nations, Rome, Italy, 2006, 4th edn, p. 97.

28 J. N. Lehto, M. Larsen, H. Zhang, N. R. Glud and W. Davison, A mesocosm study of oxygen and trace metal dynamics in sediment microniches of reactive organic material, *Sci. Rep.*, 2017, **7**, 11369.

29 S. Bolte and F. P. Cordelières, A guided tour into subcellular colocalization analysis in light microscopy, *J. Microsc.*, 2006, **224**(3), 213–232.

30 C. Moens, D. Montalvo and E. Smolders, The concentration and size distribution of iron-rich colloids in pore waters are related to soil organic matter content and pore water calcium concentration, *Eur. J. Soil Sci.*, 2020, **72**(5), 2199–2214.

31 J. Weishaar, G. Aiken, B. Bergamaschi, M. Fram, R. Fujii and K. Mopper, Evaluation of Specific Ultraviolet Absorbance as an Indicator of the Chemical Composition and Reactivity of Dissolved Organic Carbon, *Environ. Sci. Technol.*, 2003, **37**, 4702–4708.

32 M. L. Jackson, *Soil Chemical Analysis: Advanced Course*, Winsconsin, 1975, 2nd edn, Published by the author.

33 E. Zeelmaekers, *Computerized qualitative and quantitative clay mineralogy: introduction and application to known geological cases*, KU Leuven, Faculteit Wetenschappen, Leuven, 2011.

34 N. H. Suhr and C. O. Ingamells, Solution technique for analysis of silicates, *Anal. Chem.*, 1966, **38**(6), 730–734.

35 I. C. Regelink, A. Voegelin, L. Weng, G. F. Koopmans and R. N. J. Comans, Characterization of Colloidal Fe from Soils Using Field-Flow Fractionation and Fe K-Edge X-ray Absorption Spectroscopy, *Environ. Sci. Technol.*, 2014, **48**, 4307–4316.

36 M. Ohtsubo, Interaction of iron oxides with clays, *Clay Sci.*, 1989, **7**, 227–242.

37 B. Velde and A. Meunier, *The origin of clay minerals in Soils and weathered Rocks*, Springer-Verlag, Berlin Heidelberg, 2008.

38 E. Brouwer, B. Baeyens, A. Maes and A. Cremers, Cesium and rubidium ion equilibriums in illite clay, *J. Phys. Chem.*, 1983, **87**(7), 1213–1219.

39 S. Muhammad, S. T. Hussain, M. Waseem, A. Naeem, J. Hussain and M. Tariq Jan, Surface charge properties of zirconium dioxide, *Iran. J. Sci. Technol.*, 2012, **A4**, 481–486.

40 W. Davison and H. Zhang Diffusion Layer Properties, in *Diffusive Gradients in Thin-Films for Environmental Measurements*, ed. W. Davison, Cambridge University Press, Cambridge Environmental Chemistry Series, 2016, pp. 32–65.

41 F. Degryse, E. Smolders, H. Zhang and W. Davison, Predicting availability of mineral elements to plants with the DGT technique: a review of experimental data and interpretation by modelling, *Environ. Chem.*, 2009, **6**, 198–218.

This journal is © The Royal Society of Chemistry 2026

Environ. Sci.: Nano, 2026, **13**, 1935–1947 | 1947